Journal of Materials Chemistry C

Anisothermal densification kinetics of cold sintering process below 150°C

Journal:	*Journal of Materials Chemistry C*
Manuscript ID	TC-COM-01-2020-000395.R1
Article Type:	Communication
Date Submitted by the Author:	11-Mar-2020
Complete List of Authors:	Bang, Sun Hwi; Pennsylvania State University, Materials Research Institute Ndayishimiye, Arnaud; Pennsylvania State University, Materials Research Institute Randall, Clive; Pennsylvania State University, Materials Research Institute

SCHOLARONE™
Manuscripts

Journal of
Materials Chemistry C

COMMUNICATION

Cite this: DOI: 00.0000/xxxxxxxxxx

Anisothermal densification kinetics of cold sintering process below 150°C†

Sun Hwi Bang,*[a] Arnaud Ndayishimiye,[a] and Clive A. Randall[a]

Received Date
Accepted Date

DOI: 00.0000/xxxxxxxxxx

Cold sintering is an emerging non-equilibrium process methodology that densifies ceramic powders at significantly reduced temperatures. This study proposes a fundamental framework to investigate its densification kinetics. By controlling four densification process variables including transient chemistry, sintering temperature, uniaxial pressure and dwell time, anisothermal sintering kinetics of highly densified ZnO is identified and phenomenologically modeled for its relative activation energetics.

Sintering is an important scientific and also industrial processing technique, under which thermal energy and often external pressure are used to transform powder into a solid piece with enhanced mechanical strength.[1] The fundamental driving force for sintering is the reduction of the excess free energy of the powder surface by increasing the solid/solid interface and also coarsening the grain size.[2] As the ceramic sintering generally requires high temperature above 1000°C, decreasing processing temperature is a technological and environmental challenge. However, one of the immediate advantages of enabling a low temperature process is to explore new ceramic composite designs and properties for various functional material applications.[3–5]

Among low-temperature and external pressure ceramic densification methods including spark plasma sintering[6] and hydrothermal sintering,[7] cold sintering process features materials densification in an open system[8] at significantly reduced processing temperatures, which is enabled by the presence of transient phase.[9] Several technological advantages of the cold sintering includes 1) preservation of nanocrystalline size,[10] 2) co-processing of ceramic composites,[11] 3) densification of thermodynamically metastable materials,[12] 4) fabrication of multilayer electroceramics[13] and 5) significant energy reduction.[14] Although its uniaxial pressure requirement has been occasionally regarded as a methodological limitation, the recent size scale-up cold sintering process demonstrated its promising potential in industrial implementation, which can operate below 50 MPa.[15]

Despite its scientific and technological importance, the fundamental understanding of cold sintering kinetics and densification mechanisms are still in the very early stages of investigation. Analogous to conventional sintering kinetics studies, ZnO is often employed as a model material system for the cold sintering. Its initial sintering potential was first reported in 2015,[16] and to date, a combined computational and experimental investigation showed that surface hydroxylation accelerates the dissolved Zn cation adsorption and enhances the diffusion during the cold sintering.[17] Using the grain size based sintering kinetics analysis, the apparent activation energy of ZnO grain growth was only 20% of the value observed in solid state sintering.[18] Moreover, Kelvin probe force microscopy method showed that the transient liquid accounts for generating highly defective grain boundaries, leading to reduction of the activation energy of the atomic diffusion.[19]

The core objectives of understanding sintering kinetics is to predict densification behavior under different processing conditions and to obtain a uniform microstructure at high density with controlled grain size. In solid state sintering, the constant heating rate of anisothermal sintering is known to influence on densification and grain growth behavior, where faster heating rate leads to higher densification and finer microstructure at same temperature due to increases volumetric strain rate.[20] Furthermore, non–linear sintering temperature has processing advantages for finely regulating the path of morphological change.[21] Hence, the proposed study is intended to identify anisothermal densification kinetics of ZnO cold sintering and to quantify relevant activation energy. Advancing the sintering kinetics knowledge is a necessary condition to develop a complete analytical model, which will certainly accelerate cold sintering composite materials research and application deployment.

[a]*Materials Research Institute and Department of Materials Science and Engineering, Pennsylvania State University, University Park, PA, 16802, USA*
Email: sbang@psu.edu

† Electronic Supplementary Information (ESI) available. See DOI: 00.0000/00000000.

Experimental methods

Instrumentation. For any cold sintering process, transient chemistry ($\mu(t)$), sintering temperature (T), uniaxial pressure (P) and dwell time (t) can be classified as densification process variables (Fig. S1). In order to precisely measure pellet linear shrinkage[22] and temperature at each time period, we herein presents a new engineering design for collecting the real-time temperature of the pellet during the cold sintering (Fig. S2). Instrumentation, cold sintering process (Fig. S3) and material characterization details are documented in the Electronic Supplementary Information.

Mathematical derivation

Among a few reported mathematical models of anisothermal sintering kinetics[23–26], Woolfrey–Bannister's[27] approach was employed in this study to empirically analyze activation energy of the cold sintering, which has been widely accepted to analyze sintering behaviors of ZnO.[28–31] The general kinetics equation for investigating initial stage of sintering under constant heating rate is the following:

$$\frac{d(\Delta L/L_0)}{dt} = K_0 \exp\left(-\frac{Q}{RT}\right)\left(\frac{L_0}{L}\right)^{-n} \quad (1)$$

where $\Delta L/L_0$ is the linear shrinkage, t is a total time, K_0 is either constant or proportional to $1/T$ depending on mass transport mechanism, Q is the apparent activation energy, R is the ideal gas constant, T is the absolute temperature, and n is usually associated with a constant determined from a relatable sintering mechanism. By assuming that the isothermal and anisothermal shrinkage rates are equal and $Q >> RT$, Eq. 1 is approximated by:[32]

$$\left(\frac{\Delta L}{L_0}\right)^{(n+1)} = \left(\frac{K_0 R T^2 (n+1)}{\alpha Q}\right)\exp\left(-\frac{Q}{RT}\right) \quad (2)$$

where α is a constant heating rate defined as $\alpha = \frac{dT}{dt}$. After further mathematical simplifications, Eq. 1 is often used in a following form:[27]

$$T^2 \frac{d(\Delta L/L_0)}{dt} = \left(\frac{\alpha Q}{(n+1)R}\right)\left(\frac{\Delta L}{L_0}\right) \quad (3)$$

Assuming that Q, n and α are invariant during the anisothermal, taking the natural logarithm of Eq. 2 leads to determine n:

$$\ln\left(\frac{\Delta L}{L_0}\right) = -\frac{1}{(n+1)}\ln\alpha + \frac{1}{(n+1)}\left[\ln\left(K_0 R T^2 (n+1)\right) - \ln Q - \frac{Q}{RT}\right] \quad (4)$$

One of significant advantages of the proposed anisothermal kinetics approach is the direct empirical constitutive relation among linear shrinkage, temperature and time without assuming the values of exponents based on a single diffusion mechanism. However, a crucial assumption for the proposed method is that linear shrinkage is a consequence of material densification, not by liquid evaporation, which is verified to be a negligible volume fraction during the cold sintering process.

Results

Anisothermal sintering of ZnO. The relative density evolution[33] and specific surface area reduction[28] during the anisothermal

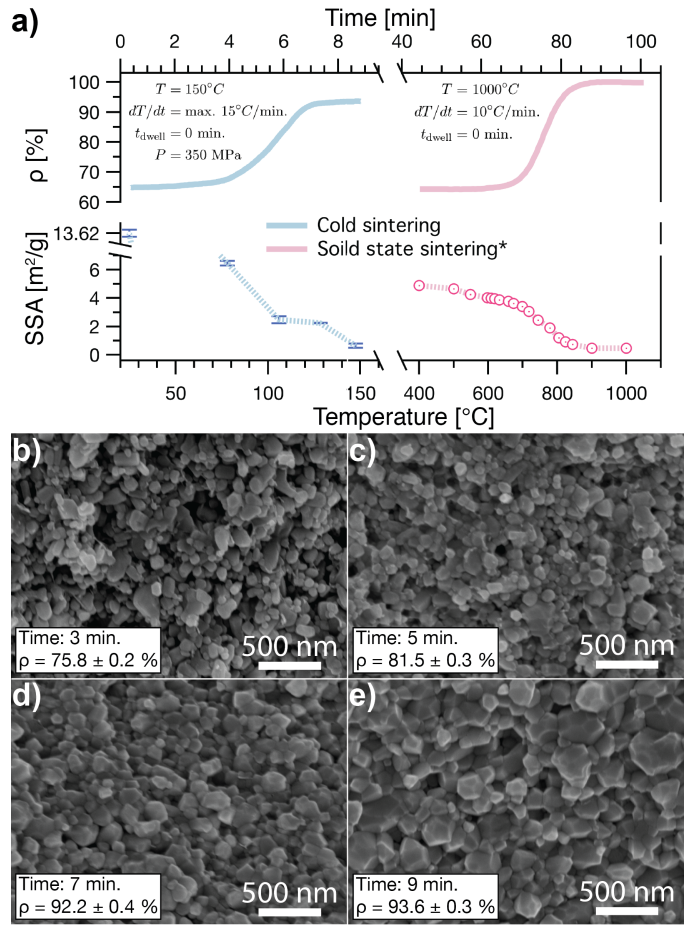

Fig. 1 Anisothermal sintering of ZnO powder under 350 MPa uniaxial pressure. a) Comparisons to ZnO solid state sintering on relative density (ρ)[33] and specific surface area (SSA)[28] in functions of temperature and time. b–e) Microstructure evolution of the fracture surfaces at the times of 3, 5, 7 and 9 minutes.

ZnO cold sintering resembles the basic shape form of the higher temperature solid state sintering process (Fig. 1a). By assuming no powder extrusion and no radial pellet shrinkage taking place during the cold sintering, the relative density can be directly projected from the linear shrinkage and initial/final relative densities. As ZnO cold sintering employs acetic acid solution as a transient phase in an open system, allowing it to mostly evaporate during the heating ramp, the rapid linear shrinkage between 3 and 6 minutes may be recognized as combined effects of powder densification and liquid evaporation. However, as thermal gravimetric analysis (TGA) of the wet green body showed that the weight loss was only 3% of the total weight up to 120°C (Fig. S4), despite the initial 15 wt.% of the added transient phase. Hence, the TGA result indicates that following points; 1) excessive transient liquid can be extruded from the wet green body during the 5-minute pressure stabilization prior to the cold sintering (Fig. S5) and 2) liquid evaporation can be considered as only a minor effect for the linear shrinkage, as the remining liquid will be likely located in the pore spaces between particles.

Chemistry during the anisothermal sintering. The microstructural evolution verified that fracture surfaces became significantly less

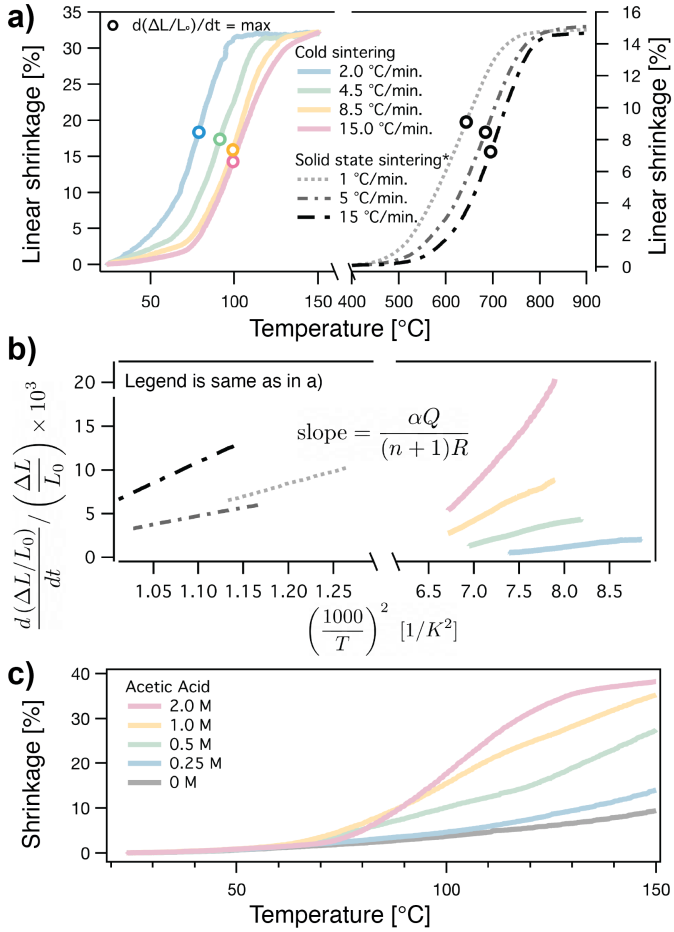

Fig. 2 a) Linear shrinkage of ZnO cold sintering under 175 MPa and solid state sintering[30] at different heating rates, where the circle shows the maximum shrinkage rate. b) Plotting based on Eq. 3, where the slope contains the activation energy term. c) Linear shrinkage dependence on concentration of the transient chemistry.

porous and particles underwent more coarsening as the cold sintering progressed (Fig. 1b–e), where the 9-minute sample's microstructure, density and specific surface area sufficiently implied that the sintering process is already in a final stage. Regarding the phase purity through X-ray diffraction (Fig. S6), zinc acetate complexes are a result of dissolution of zinc oxide powder and acetic acid solution. At elevated temperature, water begins to evaporate, the hydrate becomes anhydrous, and the following reactions may explain different pathways leading to the formation of phase pure ZnO:[34–36]

$$Zn(CH_3COO)_2(s) \xrightarrow{147-250\,^\circ C} ZnO(s) + (CH_3COO)_2O(g) \quad (R1)$$

$$(CH_3COO)_2O + 4O_2 \longrightarrow 4CO_2 + 3H_2O \quad (R2)$$

$$Zn(CH_3COO)_2(s) + H_2O \xrightarrow{147-250\,^\circ C} ZnO + 2CH_3COOH \quad (R3)$$

Here, R1 describes the decomposition of zinc acetate into ZnO and acetic anhydride, which further reacts with oxygen to produce CO_2 and H_2O as shown on R2. R3 is reported for a case of high humid atmosphere where zinc acetate can react with water to form ZnO and acetic acid. Both reactions hold reasonable for given the cold sintering, as its open system characteristic makes accessible to oxygen and water. Considering pressure solution creep mechanism as a governing mechanochemical process for the cold sintering,[37] the dissolution of ZnO by acetic acid solution may produce zinc acetate complexes at the compressional grain boundaries,[38] which is consistent with XRD analysis. Once those complexes precipitate at tensional sides, then they undergo decomposition and produce ZnO, which mainly contributes ZnO cold sintering to be phase pure.

Quantifying sintering activation energy. Linear shrinkage at different heating rates of the cold sintering and solid state sintering[30] were plotted (Fig. 2a). The corresponding temperature of the maximum linear shrinkage rate shifts towards a lower region for both sintering methods, which can be related to heating rate dependent kinetic processes.[39] Especially for the cold sintering, as a slower heating rate can retain the transient phase longer, allowing a higher degree of solution–assisted particle rearrangement, more linear shrinkage was then measured at temperature below 65°C. Regarding anisothermal sintering activation energy estimation, the modified Woolfrey–Bannister method takes the data–driven approach based on Eq. 4 to empirically determine n and its relevant uncertainty (Fig. S7). It also needs to be noted that the shrinkage behavior can be roughly classified into three parts based on shrinkage rate, and only the middle portion, featuring the maximum shrinkage rate, was considered in this proposed analysis. Analogous to the solid state sintering case, that steep shrinkage is mainly related the densification during the cold sintering as the relative density evolves up to 93%. Therefore, the proposed method focuses on quantifying activation energy of anisothermal sintering, where powder densification generally happens. According to Eq. 3, the slope contains heating rate (α), experimental exponent (n) and activation energy (Q) (Fig. 2b), and final values are summarized in Table 1. For the cold sintering, Q converges around 49 kJ/mol, where the highest heating rate has diverging and higher Q, which may be related to the reduced degree of dissolution process, as the transient phase stays shorter in the system. In comparison, the solid state sintering shows that the slowest heating rate completely diverges from other two heating rates, which are within uncertainty range. Perhaps, such a low heating rate can provide sufficient thermal energy to drive grain coarsening through surface diffusion mechanism at low temperature region, also leading to decrease in surface area and thermodynamic driving force for sintering.[39] Or, that specific heating rate may contain a possible experimental artifact as the shrinkage slope evolution is slightly aberrant from other two rates.

Table 1 ZnO anisothermal sintering activation energies at different heating rate, based on the modified Woolfrey–Bannister method.

	Cold sintering		Solid state sintering	
n	9.09 ± 1.32		13.18 ± 4.01	
Q [kJ/mol]	2.0°C/min:	48.7 ± 6.3	1°C/min:	3370 ± 950
	4.5°C/min:	47.1 ± 6.1	5°C/min:	454 ± 128
	8.5°C/min:	51.4 ± 6.7	N/A	
	15.0°C/min:	67.8 ± 8.8	15°C/min:	376 ± 106

Shrinkage depending on transient chemistry. Depending on the concentration of acetic acid, the linear shrinkage can be signif-

icantly changed (Fig. 2c), confirming that compatible transient chemistry is a key factor that enables any cold sintering process and mainly determines anisothermal sintering kinetics.

Discussion

Classifying stages of the anisothermal sintering. Considering the slope change of the ZnO cold sintering shrinkage curves, at least three different dominant processes can be hypothesized, which include 1) solution–assisted particle rearrangement, 2) powder densification by pressure solution creep and 3) grain growth and pore removal (Fig. S8). Such a claim can be considered as logical, as rearrangement will initially occur with the presence of uniaxial pressure and liquid phase in the system, but eventually stops due to the loss of the liquid and the formation of coarse grains, making less likely to continue the particle sliding.[40]

Phenomenological approach to investigate kinetics. The proposed empirical method presents a fundamental framework to study anisothermal sintering kinetics, purely based on experimental data by controlling the heating rate. Unlike the predetermined exponent with a corresponding diffusion mechanism, convincing physical interpretation of empirical n is not yet available. However, the concentration dependent shrinkage study indicated that n is indeed associated with the chemical activities of the transient phase. To the best of our knowledge, once more information on empirical n values of different materials and process conditions are accumulated, then it will be possible to find their implication as a characteristic value. Moreover, it needs to point out that the original Woolfrey–Bannister method does not take external pressure into account, but using the empirical exponent may allow to reflect the convoluted effects of applied pressure and resulting chemical activity.

Possible deviation from Arrhenius behavior. One assumption under this work and many conventional sintering kinetic studies is the temperature dependence of the rate process. As in many diffusional and chemical processes hold to Boltzmann statistical thermodynamics or Arrhenius controlled rates,[41] with its homologous temperature (T/T_m) even lower than 0.1[42] and non-equilibrium chemical dynamics,[43] there is the possible deviation from Arrhenius limit, as also outlined by Eyring and others.[44–46] One of the most well known is the Vogel–Fulcher–Tammann equation describing temperature dependence of glass viscous behavior.[47] The importance of reminding ourselves on such departures, is the fact that the relative magnitudes of the activations energies would change. Overall, more extensive data across more material system is required to consider the nature of the physiochemical mechanisms for the cold sintering.

Conclusion

Empirical approach for investigating anisothermal sintering kinetics was proposed to analyze activation energies of two different sintering methods. This work verified that the activation energy of ZnO densification is inherently small for the cold sintering process with the aid of compatible transient chemistry. The proposed fundamental framework further contributed to improving the theoretical understanding of the cold sintering process and provided reliable kinetic data, which can be potentially used in developing a relevant analytical sintering model.

Conflicts of interest

There are no conflicts to declare

Acknowledgments

We gratefully appreciate support from National Science Foundation (DMR-1728634) for enabling fundamental kinetic study. We also thank Penn State Materials Research Institute facilities and the support staff in the Materials Characterization Laboratory.

Notes and references

1 R. German, *Sintering: from empirical observations to scientific principles*, Butterworth-Heinemann, 2014.
2 J. Mackenzie and R. Shuttleworth, *Proceedings of the Physical Society. Section B*, 1949, **62**, 833.
3 M. Dürr, A. Schmid, M. Obermaier, S. Rosselli, A. Yasuda and G. Nelles, *Nature materials*, 2005, **4**, 607.
4 Y. Yong, M. T. Nguyen, T. Yonezawa, T. Asano, M. Matsubara, H. Tsukamoto, Y.-C. Liao, T. Zhang, S. Isobe and Y. Nakagawa, *Journal of materials chemistry C*, 2017, **5**, 1033–1041.
5 T. Hérisson de Beauvoir, A. Sangregorio, I. Cornu, C. Elissalde and M. Josse, *Journal of Materials Chemistry C*, 2018, **6**, 2229–2233.
6 D. Grossin, S. Rollin-Martinet, C. Estournès, F. Rossignol, E. Champion, C. Combes, C. Rey, C. Geoffroy and C. Drouet, *Acta Biomaterialia*, 2010, **6**, 577–585.
7 G. Goglio, A. Ndayishimiye, A. Largeteau and C. Elissalde, *Scripta Materialia*, 2019, **158**, 146–152.
8 A. Ndayishimiye, M. Y. Sengul, S. H. Bang, K. Tsuji, K. Takashima, T. H. de Beauvoir, D. Denux, J.-M. Thibaud, A. C. van Duin, C. Elissalde *et al.*, *Journal of the European Ceramic Society*, 2019.
9 C. A. Randall, J. Guo, A. Baker, M. Lanagan and G. Hanzheng, *Cold sintering ceramics and composites*, 2017, US Patent App. 15/277,553.
10 K. Tsuji, A. Ndayishimiye, S. Lowum, R. Floyd, K. Wang, M. Wetherington, J.-P. Maria and C. A. Randall, *Journal of the European Ceramic Society*, 2019.
11 J. Guo, B. Legum, B. Anasori, K. Wang, P. Lelyukh, Y. Gogotsi and C. A. Randall, *Advanced Materials*, 2018, **30**, 1801846.
12 S. H. Bang, T. Hérisson de Beauvoir and C. A. Randall, *Journal of the European Ceramic Society*, 2019, **39**, 1230–1236.
13 T. Hérisson de Beauvoir, S. Dursun, L. Gao and C. A. Randall, *ACS Applied Electronic Materials*, 2019.
14 T. Ibn-Mohammed, C. A. Randall, K. Mustapha, J. Guo, J. Walker, S. Berbano, S. Koh, D. Wang, D. Sinclair and I. Reaney, *Journal of the European Ceramic Society*, 2019, **39**, 5213–5235.
15 S. H. Bang, K. Tsuji, A. Ndayishimiye, S. Dursun, J.-H. Seo, S. Otieno and C. A. Randall, *Journal of the American Ceramic Society*, 2020.
16 B. Dargatz, J. Gonzalez-Julian and O. Guillon, *Science and technology of advanced materials*, 2015, **16**, 025008.
17 M. Y. Sengul, J. Guo, C. A. Randall and A. C. van Duin, *Angewandte Chemie*, 2019.
18 S. Funahashi, J. Guo, H. Guo, K. Wang, A. L. Baker, K. Shiratsuyu and C. A. Randall, *Journal of the American Ceramic Society*, 2017, **100**, 546–553.
19 J. Gonzalez-Julian, K. Neuhaus, M. Bernemann, J. P. da Silva, A. Laptev, M. Bram and O. Guillon, *Acta Materialia*, 2018, **144**, 116–128.
20 M.-Y. Chu, M. N. Rahaman, L. C. De Jonghe and R. J. Brook, *Journal of the American Ceramic Society*, 1991, **74**, 1217–1225.
21 H. Palmour, *Science of sintering*, Springer, 1989, pp. 337–356.
22 R. Floyd, S. Lowum and J.-P. Maria, *Review of Scientific Instruments*, 2019, **90**, 055104.
23 M. Gropyanov and G. Abbakumov, *Science of Sintering*, 1975, **7**, 3–15.
24 V. Ivensen and V. Belen'kii, *Powder Metallurgy and Metal Ceramics*, 1990, **29**, 611–615.
25 S. Salem and A. Salem, *Thermochimica acta*, 2014, **575**, 322–330.
26 M. Kovalchenko, Y. G. Tkachenko, D. Yurchenko and V. Britun, *Powder Metallurgy and Metal Ceramics*, 2014, **53**, 180–190.
27 J. Woolfrey and M. J. Bannister, *Journal of the American Ceramic Society*, 1972, **55**, 390–394.
28 L. Perazolli, E. Longo and J. A. Varela, *Sintering technology*, Marcel Dekker, 1996, pp. 77–84.
29 J. Han, A. Senos and P. Mantas, *Journal of the European Ceramic Society*, 1999, **19**, 1003–1006.
30 N. Neves, R. Barros, E. Antunes, I. Ferreira, J. Calado, E. Fortunato and R. Martins, *Journal of the American Ceramic Society*, 2012, **95**, 204–210.
31 T. K. Roy and A. Ghosh, *Ceramics International*, 2014, **40**, 10755–10766.

32 W. S. Young and I. B. Cutler, *Journal of the American ceramic Society*, 1970, **53**, 659–663.
33 F. Zuo, A. Badev, S. Saunier, D. Goeuriot, R. Heuguet and S. Marinel, *Journal of the European Ceramic Society*, 2014, **34**, 3103–3110.
34 A. Moezzi, A. McDonagh, A. Dowd and M. Cortie, *Inorganic chemistry*, 2012, **52**, 95–102.
35 Z. Xia, Y. Wang, Y. Fang, Y. Wan, W. Xia and J. Sha, *The Journal of Physical Chemistry C*, 2011, **115**, 14576–14582.
36 T. Arii and A. Kishi, *Thermochimica acta*, 2003, **400**, 175–185.
37 F. Bouville and A. R. Studart, *Nature communications*, 2017, **8**, 14655.
38 D. Elliott, *Geological Society of America Bulletin*, 1973, **84**, 2645–2664.
39 R. Brook, Proc. Br. Ceram. Soc., 1982, p. 7.
40 V. Skorokhod, *Powder Metallurgy and Metal Ceramics*, 1999, **38**, 350–357.
41 S. Arrhenius, *Zeitschrift für physikalische Chemie*, 1889, **4**, 226–248.
42 M. Ashby, *Acta Metallurgica*, 1974, **22**, 275–289.
43 M. Y. Sengul, C. A. Randall and A. C. van Duin, *ACS applied materials & interfaces*, 2018, **10**, 37717–37724.
44 H. Eyring, *The Journal of Chemical Physics*, 1935, **3**, 107–115.
45 V. Aquilanti, N. D. Coutinho and V. H. Carvalho-Silva, *Philosophical Transactions of the Royal Society A: Mathematical, Physical and Engineering Sciences*, 2017, **375**, 20160201.
46 V. H. Carvalho-Silva, N. D. Coutinho and V. Aquilanti, *Frontiers in chemistry*, 2019.
47 A. K. Varshneya and J. C. Mauro, *Fundamentals of Inorganic Glasses*, Elsevier, 2019.